Soft Matter

PAPER

View Article Online
View Journal | View Issue

Cite this: *Soft Matter*, 2021, **17**, 9170

Adhesion directed capillary origami†

Timothy Twohig and Andrew B. Croll *

Received 5th August 2021,
Accepted 20th September 2021

DOI: 10.1039/d1sm01142a

rsc.li/soft-matter-journal

Capillary origami takes advantage of the surface forces of a liquid drop to assemble thin film structures. After a structure is assembled, the drop then evaporates away. The transient nature of the liquid drop means that the creation of dry and stable structures is impossible. Work presented in this paper shows that adhesion is, in fact, a key tool that enables the creation of stable, complex, capillary assembled origami structures, rather than a problem to be avoided. Here, polydimethylsiloxane thin films were used in several simple experiments designed to identify the balance between substrate–film adhesion and film–film adhesion in the context of capillary assembly. We then demonstrate how directional adhesion can be used to direct film peeling in order to create non-trivial patterned folds after a fluid drop is deposited. A minimal complex structure, a "double-fold" was created to demonstrate how adhesion uniquely facilitates multiple-step capillary assembly. Finally, a familiar "origami airplane" was created with these methods, demonstrating that adhesion aided capillary origami can be used to assemble complex, functional structures.

As problems in science and engineering have become more complicated, researchers have often found success by looking for solutions in seemingly unrelated areas. Consider, for example, the significant progress made toward solving many packing and deployment problems that has been inspired by the ancient art of origami.[1–5] Traditional origami involves folding thin (two-dimensional) paper sheets into three dimensional aesthetically desirable structures. The paper structures are stable due in large part to the irreversible folds and creases created during the assembly process. Constructing the origami structures requires the repetitive application of steps such as lifting, bending, creasing, and partial unfolding of portions of a sheet. Variants of these basic steps, have lead to advances in solar cell deployments,[6,7] impact mitigation systems,[8] robotics,[9,10] batteries,[11,12] artery stents,[13] and guided assembly.[14–16]

The success of origami inspired design at the macro-scale has caused the natural progression of the technique towards the micro and nanoscales.[17–22] Downsizing is especially attractive to the medical field for the purposes of tailored drug delivery[17,23,24] and other microscopic medical devices.[13,25] However, as the sheet materials are scaled down new difficulties arise due to the increased importance of surface interactions. In particular, adhesion due to the ubiquitous but weak van der Waals forces tends to complicate folding as contact becomes irreversible. Adhesion is ignored in macroscopic sheets because they are rigid enough that adhesive interactions lead to little deformation of the sheet and therefore little true contact between sheet surfaces. However, as a sheet's thickness, t, becomes small, sheets are more easily bent by adhesive interactions between substrates, actuators, and themselves. With respect to origami-inspired design, the consequences require that any force or object used to manipulate a micro-scale film must be strong enough to overcome adhesion, but at the same time must be gentle enough to avoid tearing or otherwise damaging the thin film. Furthermore, any manipulator used to create a particular pattern must not only firmly hold the film but also release the film on demand.

Capillary forces have offered an interesting solution to some of the issues of manipulating and joining materials at the micro and nano-scale.[21,26–28] In the so called 'capillary origami' process a thin film is cut to a desired shape and then laid on an adhesion free substrate. Placing a liquid droplet on the film drives folding as the surface tension of the drop draws the thin film upwards and around the volume of the drop.[26] Most commonly the fluid is water due to its relatively high surface tension, however, liquid metal can also be used to actuate thin plates.[17,29,30] Often, actuation points (hinges) are designed into the film to enable more localized bending and sharper origami-like geometric structure.[17,29–33] When the drop evaporates, no residue is left behind and the film relaxes back to its initial state, unharmed. Capillary origami has thus far allowed the creation of many geometries, especially polyhedra,[17,26,29,30] but it still fails to achieve the full potential of origami designs. This is because complex, bistable origami structures require

Department of Physics, North Dakota State University, Fargo, USA.
E-mail: andrew.croll@ndsu.edu; Tel: +1-413-320-3810

† Electronic supplementary information (ESI) available: Details of calculations, and additional discussion and movies of assembly processes. See DOI: 10.1039/d1sm01142a

multi-step assembly processes which cannot be achieved with a single fluid drop.

Closely examining the steps for the creation of an origami model reveals that repetition of only two actions are needed to create a non-trivial sculpture: (1) a force is applied such that it causes a film to lift from a substrate and to bend. (2) The bend is held in place (creased) enabling additional steps to occur.[34] Using paper origami as an example, the first step involves the artist's fingers and the second step is accomplished by fingers driving the curvature to localize and create a plastic defect (a fold). Careful alignment of where folds are placed and repetition opens the door for a multitude of origami shapes. Unfortunately, capillary forces alone are usually insufficient to create plastic damage in a sheet.

In this work we explore how adhesive forces, which are typically removed in order to enable capillary origami, are in fact the key tool needed to overcome the limitations of single-step capillary driven origami assembly. We conduct simple experiments to show how and when capillary forces can become strong enough to peel a film from a substrate (see Fig. 1 and 2). We show how self-adhesion represents a new mechanism that can be used to 'fix' sharp bending in a desired position. We note the importance of peel-mechanics in both of these processes, and show how the peel front (crack tip) can be guided with textured substrates to facilitate finer control of the process. We demonstrate that higher order structures are made possible by adhesive elastocapillary control by combining peel front guiding between a film and substrate and staged delivery of water drops. Finally, we use the technique to assemble a prototype 'complex' origami: a "paper" airplane.

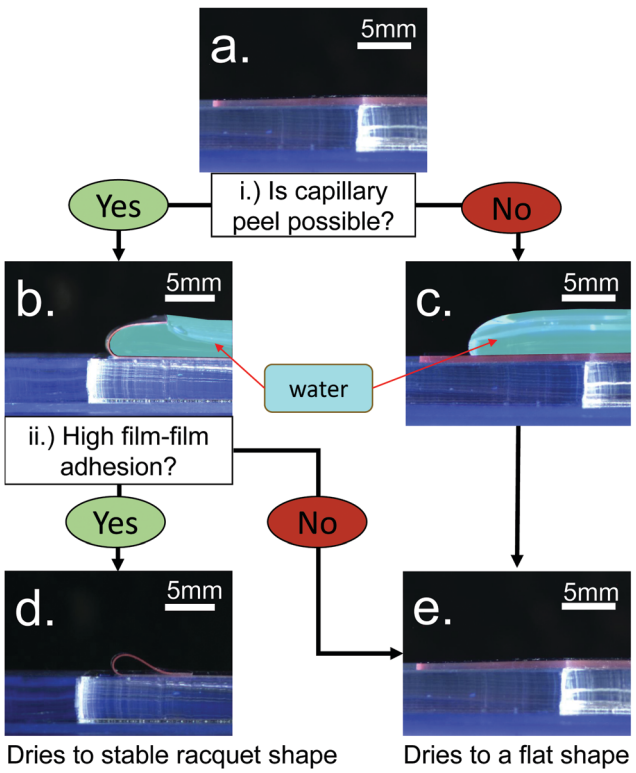

Fig. 1 Possibilities for a thin-film capillary origami system. A film resting (a) has a drop of water added to it. If the capillary forces are greater than the adhesion forces, peel is possible (b). If peel is not possible, the film will remain in the flat state while the drop slowly evaporates (c) and will remain flat when the drop completely dries (e). Films that did peel form a bent shape around the droplet which persists as the drop dries, but slowly takes on a higher radius of curvature. If the film is long enough it will eventually come into self-contact. If self-adhesion is strong enough the film will retain a racquet shape indefinitely (d), otherwise it will open in order to reduce bending energy and relax to a dry, flat final state (e).

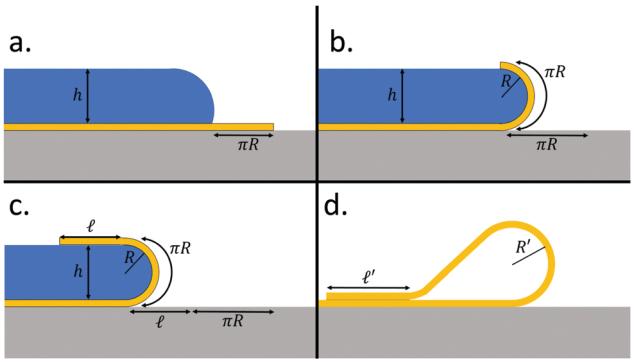

Fig. 2 Illustration of capillary peel for a water–PDMS film system. (a) Water is placed on a flat film and the upward capillary forces of the water pull on the film. As the water approaches the edge of the film, the upward forces are larger than the forces keeping the film in place and the film will detach from the substrate. For convenience in the scaling argument, we imagine the drop at rest at a position some small distance from the film edge such that the 'free length' of film is just enough to bend around the drop as in (b). Note that the water does move closer to the film edge in reality. (b) The detached film will be pulled along and up the surface of the water drop, acting to cover the greatest amount of liquid as possible. (c) Once a full 180° bend is created, there is a runaway rolling capillary peel front causing more of the water surface to be covered by film. This will continue until the peeling is stopped by some other interaction or limit. (d) If enough of the film has capillary peeled to allow for large film–film adhesion to be created after the film dries, the remaining shape is known as the "racquet" shape.

1 Experimental

1.1 Thin-film preparation

Thin films were created from Sylgard 184 polydimethylsiloxane (PDMS) at a weight ratio of 10 : 1 (prepolymer to crosslinker) according to the following protocol. First, prepolymer and crosslinker is measured at a 10 to 1 weight ratio and mixed thoroughly. The mixture is then degassed in a vacuum oven. Next, the uncured PDMS was coated onto polyacrylic acid (PAA) coated glass slides and placed onto a spincoater (Laurell Technologies Corporation Model WS-400BZ-6NPP/LITE) and quickly rotated to create a thin, uniform film on the slide. PDMS films created by spin coating were on the order of tens of microns in thickness. Thicker samples (over a hundred microns in thickness) were created by drop-casting uncured PDMS onto a PAA coated glass slide.

The film samples were then placed in a vacuum oven at a vacuum pressure of 25 inHg for approximately 20 minutes to remove any air bubbles incurred during the casting process.

Samples were then annealed at 85 °C for 90 minutes. Samples were allowed to cool and then scored into strips 1 cm by 3 cm, with longer samples occasionally being created to test the effects of sample length. Samples were submerged in MilliQ (Millipore Inc) filtered water to dissolve the PAA release layer and allow the film to float to the top of the container. Floating films were gently placed onto kimwipes to dry overnight in a closed container.

Thickness values for each sample were determined using three-dimensional scanning confocal microscopy (Olympus FLUOVIEW FV1000). Thickness measurements were conducted after capillary experiments were completed. Each film sample was placed on a glass slide and the height of the film from the glass surface was scanned at three locations around the perimeter. The average was reported as the thickness.

1.2 Substrate preparation

Moulds for substrates were created by hot-pressing a glass pattern into a polystyrene (PS) plate. Hot pressed PS moulds were ready to use after cooling, cleaning, and drying.

Additionally, 3D printed moulds were created using Formlabs clear photopolymer resin in a Formlabs form2 3D printer. Substrates were designed to have a repeating pattern with cross-sectional slices of cusp, circular, or rectangular shapes as seen in Fig. 3a–c, respectively. Each shape allowed for different adhesion values to the films with the cusp shaped substrates giving values less than 3% adhesion, rounded substrates giving around 5–15% adhesion, and rectangular substrates for approximately 20–95% adhesion compared to a flat piece of PDMS. As discussed below, the altered adhesion is due only to altered contact area between film and substrate. Raised features were 1–2 mm in height with a repeating period of 1–2 mm. All 3D printed moulds were prepared for patterning of PDMS by placing the mould in a bath of isopropyl alcohol and agitating two minutes, then resting in the bath for ten minutes. The mould was then allowed to dry in the air for at least 24 hours. Moulds were then soaked in filtered MilliQ water for 2 hours, rinsed, and placed into an oven at 85 °C for 24 hours. The moulds were allowed to cool, then washed with detergent and water, rinsed with MilliQ water, and allowed to dry. Cusp-shaped moulds were then ready to be used to directly create PDMS substrates, since the roughness of the printed surfaces lowered adhesion as was desired. Rectangular moulds were printed too rough to create adhesion at the values desired, so these moulds were sanded to remove large roughness features, and then coated with a solution of PS in toluene and allowed to dry to create a smooth surface. These moulds were then used to create a 10 : 1 PDMS negative.

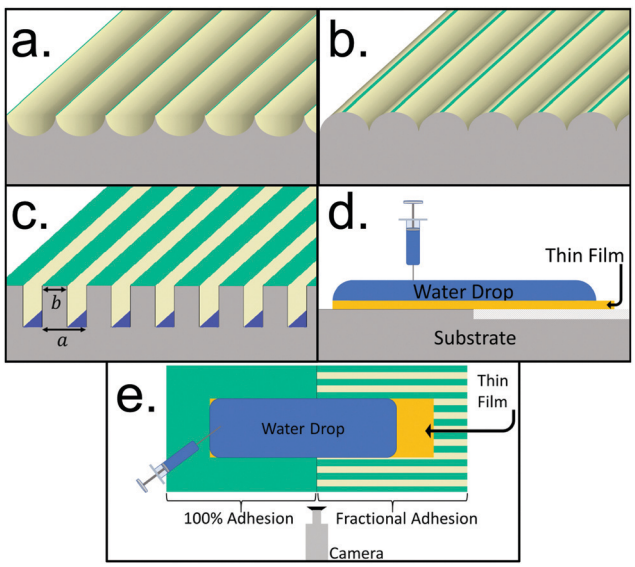

Fig. 3 Experimental setup of the film, substrate, water drop and application, and camera setup. (a) Cusp-shaped substrates used for the lowest adhesion to the film. (b) Rounded substrates giving adhesion values of 5–10% to the film. (c) Rectangular substrates for adhesion values of 20–90% to the film. Raised areas that adhere to the film are colored in green to show relative adhesion. (d) Side profile of the experimental setup. Water drop placed on the film which is adhered to the substrate. Substrate may consist of two different adhesion values to force peeling to only occur at one end of the film. (e) Top view of experimental setup, showing two film–substrate adhesion areas and how the direction of peeling is parallel to the direction of the substrate pattern.

The PDMS was prepared with the same procedure outlined above for the thin films, but after the 10 : 1 mixture was poured into the mould, the degassing process was cycled twice though 5 minute vacuum depressurizations and once through a 20 minute depressurization. All depressurizations were brought to 25 inHg and held for the set amount of time to ensure PDMS would reach all parts of the mould, then put in an oven set to 85 °C for 90 minutes. After cooling, substrates and negatives were gently peeled out of the moulds and placed pattern side up on glass slides. Negatives were placed in a UVO Cleaner (Jelight Company Inc. Model No. 42A) and oxidized for 35 minutes. After cooling, these negatives were used as moulds to create 10 : 1 PDMS substrates.

1.3 Capillary peel experiment

Dry sample films were placed onto substrates so that the long axis of the film was parallel to the ridges patterned on the substrate (Fig. 3d and e). Films were arranged so that a length of many times the elastocapillary length $\left(L_{ec} = \sqrt{\frac{B}{\gamma_{lg}}}\right)$ was adhered to the patterned portion of the substrate in order to ensure that if capillary peel and bending were possible, a film is able to achieve a full 180° bend. The opposite end of the film was adhered to an unpatterned portion of substrate (Fig. 3d and e). This was done to ensure that capillary peel would occur at only the end of the film with the lower substrate adhesion which prevents the scenario in which symmetric film peeling occurs and film ends interfere with one another. Ten to thirty minutes after placing the film on the substrate, the film–substrate adhesion was imaged near the intended fracture edge by optical microscopy. Images were taken from above, near the peeling edge, with an Olympus BX51 upright microscope at 5× magnification. Pictures were later analyzed in order to determine the true fraction of film–substrate contact area using

ImageJ image analysis software. These values were reported as k, the fraction of contact area to total film area. Note that no attempt was made to estimate any strain energy stored in the film as it contacts the substrate. Strain was assumed to be negligible compared to the other energies present in the problem. The lowest adhesion samples were created by applying a nonstick coating to the underside of the film. When there was no film–substrate adhesion visible using microscopy, an adhesion value of $k = 0.0001$ was assigned, representing a lower limit of what is observable with this method (zero contact is physically impossible).

Next, the samples and substrates were placed on a stage and a side-on picture of the profile was recorded by a camera (Fig. 3d and e) every few seconds. MilliQ filtered water was placed onto the center of the sample and allowed to spread to the edges. If the water caused the film to peel and fully bend onto itself, water was added until all of the remaining flat film was covered, then the water was removed by evaporation or syringe. Films that did not fully peel and bend had water added until all of the flat surfaces were covered, creating a large ''pancake'' drop resting on the film. Water was then slowly removed, while the peel edge was observed carefully for signs of capillary peeling and bending. Samples were removed from substrates and allowed to dry. Clean substrates were reused until changes in the fraction of adhesion were observed.

1.4 Racquet stability experiment

The ''racquet shape'', shown in Fig. 2d, is the geometry which occurs when a thin film is adhered to itself and placed on a substrate. It is often modeled as an elastica, and has been explored theoretically by several researchers.[26,35–38] Experiments to determine the stability of a ''racquet'' structure created by capillary peeling a thin film from a substrate and then allowing the water to dry were conducted in a manner similar to the capillary peel experiment. A thin film was placed on a substrate split into two adhesion zones. The ''adhesion zone'' was nearly 100% adhered to the film and the other ''non-adhesive zone'' was a very low adhesion value substrate (1%), identical to the setup in Fig. 3d and e. A top down picture of the setup was taken to record the length of the film extending into the non-adhesive zone from the edge of the adhesion zone. This was recorded as the free length of the experiment. Following the steps illustrated in Fig. 2, water was added to the top of the film and then removed to lift and roll the film's edge in the non-adhesive zone onto the flat film in the adhesive zone.

In the case where a film did not capillary peel, the free edge was lifted and placed upon the top of the water puddle at a 180° bend, further peeling to the adhesive edge was facilitated by the capillary puddle. These samples were noted as ''forced peel'' samples. The water was then allowed to dry, leaving either a stable racquet shape or a film that relaxed back to its flat state without the capillary drop present, represented in the final states in Fig. 1. These final states were recorded. The free lengths were adjusted and the experiment was repeated several times with films of the same thickness.

1.5 Double-fold experiment

An experiment to create a multi-step, double fold structure was also conducted, following a modified repetition of the procedure of the capillary peel experiment described above. The major modifications were to arrange a square film on a patterned substrate so that only one-quarter of the film was on an unpatterned substrate and fully adhered (lower-left quadrant in Fig. 8a). Second, two very low adhesion patterns were placed so that their axis was 90° to a final low adhesion (bottom right in Fig. 8a) quadrant. This substrate design (top-down schematic in ESI†) ensured that water added to the center of the square film would create a fold running horizontally along the middle of the film, where the peel front would stop upon encountering high adhesion along its length as it encounters the two higher adhesion quadrants. This first water drop was then allowed to dry. A second water drop was deposited from the center of the folded rectangular film and caused a secondary peel of the film from the remaining lower adhesion quadrant. Ultimately, this left only the lower-left quadrant anchored to the substrate and the peeled film folded into a small square shape on top of that section. The sequence of events is shown in Fig. 8 (timelapse video available in ESI†).

1.6 Adhesion measurements

Adhesion measurements for the PDMS film and PDMS substrate interfaces were measured with the same procedure and setup as is outlined for macroscopic films by Elder *et al.*[39] A top and bottom plate were coated with PDMS and a drop coated film was bent between the two plates in a ''tape loop'' geometry. The film was prepared with the same drop-casting procedure as described above for creating thin PDMS films. The PDMS-coated plates were prepared in the same manner as the drop coated films, except that the PAA release layer was not used, meaning that the PDMS has likely bonded to the glass slide during curing. The top plate's position was cycled, first compressing the tape loop past the elastocapillary length of the system, L_{ec}, then relaxing back to the starting point. The cycle was then repeated several more times. The force from the tape loop on the bottom plate, the separation distance of the two parallel plates, the speed of plate movement, and the width of the film loop were all recorded. The force difference between the compression and relaxation curves was used with these measurements to find the PDMS–PDMS adhesion value. See ESI† for details.

2 Results and discussion

2.1 Capillary peel and substrate-adhesion fraction

When a drop of fluid is placed on a thin film, it will spread out to reach the advancing contact angle permitted by the system's Young–Laplace balance (θ_e). If that contact point is far from the edge of the film it is unlikely for the drop to cause the film to peel and lift from a substrate due to the overall weight of the film and the increased in-sheet stretching cost required to form a circular ridge around the droplet. Even if the ridge is only

transient, the Gaussian curvature will change from the flat state and a stretching cost must be exceeded for any peeling to occur. On the other hand, if the droplet reaches the edge of a film, it is likely to be pinned there by defects. This means that the contact angle is not likely to remain in equilibrium and the drop is likely to spread out along the edge flattening the formerly circular contact line and allowing bending to occur.[40] The weight of the film to be lifted is minimized and, more importantly, any changes to the Gaussian curvature at the front are avoided. This is the most likely case for capillary peeling to occur and what we focus our experiments on.

For a film to peel from a substrate two things must happen. First, the capillary force of the drop must exceed the work of adhesion between the film and the substrate on which it rests. In fact, due to losses which occur during the propagation of the interfacial crack (the peel front) the true work of adhesion can only be considered a lower limit for the process.[41,42] Secondly, the bending cost of the film must be smaller than the difference between the work of adhesion and the capillary force. If the former is not true, there is no drive for the system to lift from the substrate. If the latter is not true observation would not be able to determine that the film edge is not adhered to the substrate (as it would not be lifted and the film as a whole cannot hover).

Capillary peel experiments were performed in order to study the basic ability of a fluid drop to peel a film from an adhesive substrate. In these experiments, the film thickness was varied in order to alter bending energies and the fraction of the film adhered to the patterned substrate was varied in order to alter the system's work of adhesion while keeping interfacial chemistry constant. In this manner, a state diagram can be constructed as shown in Fig. 4. Here blue solid circles are used to show experiments where capillary peel was observed (where the fluid could bend the film 180°) and light blue open squares represent the combinations where no peeling from the substrate was observed. As might be expected, the experiments that showed complete film folding tended to be the thinnest films with the least adhesion to the substrate.

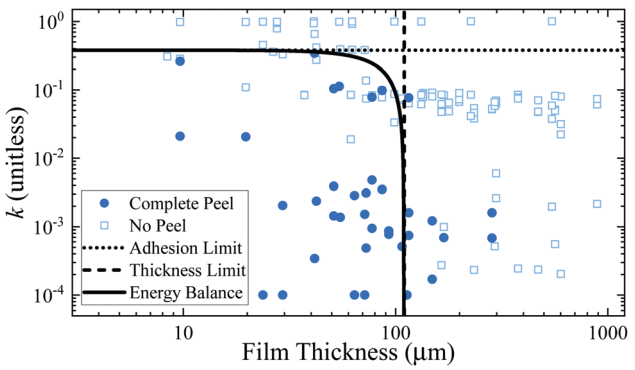

Fig. 4 A plot comparing the fraction of the thin-film adhered to the substrate (k) against the thickness of the film. The color of each data point represents if the film was observed to peel from the substrate when a water drop was placed on top of the film. Blue circles represent films of a given thickness that capillary folded (bent 180°) and peeled from a given substrate. Light blue open squares represent combinations where no capillary peeling was observed. The horizontal dotted line illustrates the cutoff line above which surface energies do not allow peeling. The vertical dashed line represents the maximum thickness film that could be bent around the water puddle. The solid line shows the full balance of surface and bending energies. Films that exist below the solid line can be expected to peel.

Fig. 4 suggests an apparent upper limit for the fraction adhered to the substrate with the highest observed capillary peel occurring at $k = 0.34$. Capillary peel reliably occurs when fraction adhered is below $k = 0.10$. As the thickness of a film increases, the limiting adhesion values for capillary peeling decrease. This trend continues until film thickness of approximately 250 μm are reached (the thickest capillary peel is observed in a film of thickness 285 μm). Above this film thickness value, the capillary drop cannot peel and fold the PDMS film.

A simple scaling argument can be constructed by considering the free energy before and after wrapping. The basic geometry is shown in Fig. 2a–c. Note that the figure shows the drop a small distance from the end of the film. In reality the drop will usually reach near to the film edge before folding occurs. The length in the schematic is a convenience, because it enables the drop to be considered stationary. The drop is large but not infinite, so if it reaches the film edge and then is wrapped by the film, its center of mass would have to move during wrapping. Before a film is lifted from a substrate, in the limit of a large droplet, the systems energy is given by

$$\frac{U_1}{b} = \pi R(\gamma_{la} + \gamma_{fa} + \gamma_{fs}) + \frac{1}{2}\rho g h^2 L, \quad (1)$$

where the γ values represent the surface energy of an interface and the subscripts of f, s, a, and l correspond to the film, substrate, air, and liquid surfaces, respectively. ρ is the fluid density L is the horizontal extent of the droplet, and b is the length of the contact line (out of page dimension of the film shown in Fig. 2). Though not necessary, we assume the radius of curvature, R, scales as $h/2$ for simplicity. We further assume that h is unchanged after wrapping, which is true if the drop volume is large and the film thickness is relatively small.

Just after wrapping, with the same assumptions as above, the free energy is altered to

$$\frac{U_2}{b} = \pi R(\gamma_{lf} + \gamma_{fa} + \gamma_{sa}) + \frac{1}{2}\rho g h^2 L + \pi B/2R, \quad (2)$$

with the bending modulus given by $B = Et^3/12(1 - \nu^2)$ where E is Young's modulus and ν is the Poisson ratio. Hence the change in energy due to wrapping is,

$$\frac{\Delta U}{b} = \pi R(\gamma_{lf} + \gamma_{sa} - \gamma_{la} - \gamma_{fs}) + \frac{\pi B}{2R} \quad (3)$$

The energy difference can be used to determine the function $k(t)$ that delineates the boundary between successful capillary folding and unsuccessful folding.

Before determining the full function, it is instructive to explore two limiting cases. First, if a film is infinitely thin the bending cost can be ignored, and the final term in eqn (3) can be dropped. ΔU must be less than zero in order for wrapping to

occur spontaneously, and a critical γ_{fs} can be determined. In our experiment we note that $\gamma_{sa} = \gamma_{fa}$ and can rewrite the film substrate energy as $\gamma_{fs} = k\gamma_{ff} + 2(1 - k)\gamma_{fa}$ as the substrate material and film material are identical by design. Setting $\Delta U = 0$ allows a limiting k to be determined:

$$k_{t\to 0} = \frac{\Delta\gamma'}{\Delta\gamma} \tag{4}$$

where $\Delta\gamma$ is the work of adhesion between the substrate and film ($\Delta\gamma = 2\gamma_{fa} - \gamma_{ff}$) and $\Delta\gamma'$ is the equivalent term for the water/film interface ($\Delta\gamma' = \gamma_{la} + \gamma_{fa} - \gamma_{lf}$). In our experiments, surface energy values give a $k_{t\to 0}$ value of 0.38.[43–45]

The maximum adhesion percentage predicted by eqn (4) is indicated by the dotted horizontal line in Fig. 4 and shows good agreement with the apparent transition between peeling and non-peeling states in low thickness films. As the film thickness increases, agreement is reasonable until a thickness of approximately one hundred micrometers. Here the limit between these two peeling states begins to fall from the zero-thickness prediction.

A second limit can be determined by considering a zero adhesion limit which would correspond to the work of adhesion falling to zero ($\Delta\gamma \to 0$) or equivalently in our experiment $k \to 0$. In either case, eqn (3) reduces to

$$\frac{\Delta U}{b} = -\pi R\Delta\gamma' + \frac{\pi B}{2R}. \tag{5}$$

and the limiting thickness can be written as

$$t_{\Delta\gamma\to 0} = \left[\frac{24R^2\Delta\gamma'(1-\nu^2)}{E}\right]^{\frac{1}{3}} \tag{6}$$

In simpler terms, the critical thickness is related to a balance between the elastocapillary length $\left(L_{ec} = \sqrt{B/\Delta\gamma'}\right)$ and the capillary length $\left(\kappa^{-1} = \sqrt{\gamma_{la}/\rho g}\right)$.[27,46] The driving force must be able to bend the film around the droplet, the height of which is determined by the capillary length. This is an important design consideration if driving fluids are exchanged, density as well as surface tension are important.

Explicitly, the drop height is expected to be

$$h = 2\sqrt{\frac{\gamma_{la}}{\rho g}}\sin\left(\frac{\theta_e}{2}\right), \tag{7}$$

where θ_e is the equilibrium contact angle of the fluid on the (flat) film.[46] With the surface energies relevant to our experiment, we calculate a height of 3200 μm and a thickness limit of $t_{\Delta\gamma\to 0}$ = 110 μm.[43–45]

The thickness limit is shown as a dashed vertical line in Fig. 4, which agrees reasonably with the majority of the data, though films over 2 times as thick were observed to fold. We believe the discrepancy lies in dynamics between the film and droplet that were not controlled precisely enough in our experiments and not considered in the scaling model. For example, if an interfacial crack begins in a film corner (where b is effectively smaller) or on a defect in the pattern, it may be able to propagate more easily. There may be additional details due to the approximations of considering the system 2D. In reality, the fluid has curvature in other directions which are ignored in this model. Furthermore, there is no consideration of exactly how the crack between film and substrate is nucleated in our model.

Finally, we solve eqn (3) directly and plot the full boundary as a solid line in Fig. 4, which is determined to be

$$k(t) = -\frac{\Delta\gamma'}{\Delta\gamma} + \frac{E\rho g}{24(1-\nu^2)\Delta\gamma\gamma_{la}\sin^2(\theta_e/2)}t^3. \tag{8}$$

Eqn (8) smoothly connects the two limits discussed above, and forms a good guideline for understanding substrate adhesion in the design of capillary origami systems.

2.2 Guiding a capillary peel front

One aspect of capillary peel which has been overlooked up to this point, is the ease at which the direction of a peel front can be controlled with patterned interfaces. Once capillary forces have initiated a peel, a film will typically peel until the driving droplet is covered. However, if the work of adhesion is altered locally this need not be the case. This is an important feature because a substrate can then be used to determine the final position of a pivot point or fold. In our experiment, this can easily be accomplished through a change in pitch, or pattern orientation. Consider a substrate which is designed with two different regions of pattern. In the first region the long parallel channels of the substrate are orthogonal to the (assumed) peel direction of the film (Fig. 5a), but in the second the pattern is rotated by 90° (Fig. 5b). The substrate will allow a crack to propagate in region one but will cause the crack to stop in region two. This is because the quasi-one dimensional contact line will interact with the surface and 'feel' the average k along its length. When the peel front is orthogonal to the pattern (Fig. 5a) it experiences a low k because the contact line touches the substrate at several points – the contact line does not touch a continuous region of substrate (regions touching substrate and regions over a gap are averaged together). When the peel front reaches the second region of substrate where the pattern

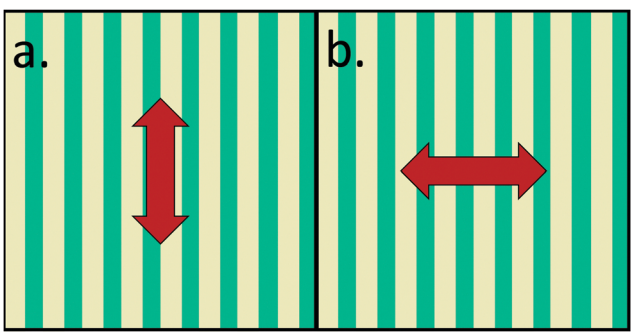

Fig. 5 Schematic of patterned substrates. In (a) a film will continuously peel in the direction of the arrow because the peel front experiences a constant value of adhesion (in this figure approximately 50%). While a peel initiated in the direction of the arrow in (b) will alternate between periods where there is no adhesion and 100% adhesion, depending on if the front is crossing a raised or lowered section of the substrate.

is now parallel to the front (Fig. 5b), it will experience $k = 0$ if it is over a gap, but will experience $k = 1$ when it reaches the portion of pattern which touches the film. Here the line will not average the contact and noncontact regions, but experiences each separately.

Manipulating the films and peel fronts using thin strips allows peel to be guided in useful directions. Further examples of how thin strips of adhesive substrate can act to stop or to guide peeling are present schematically in Fig. 6 and experimentally in Fig. 8 discussed below. Fig. 6 demonstrates several orientations in which a crack can be arrested, but also shows how a front can be directed to fold in different directions.

Finally, we point out how patterned substrate blocks can be used much like typesetting. Different patterned blocks (characters) can be arranged side by side to create the desired overall substrate. For example, pattern free blocks can be arranged to stop bends, patterned regions where peeling in a certain direction is desired and so on. Once such a 'character set' is developed, endless arrangements, and thus endless fold patterns are possible.

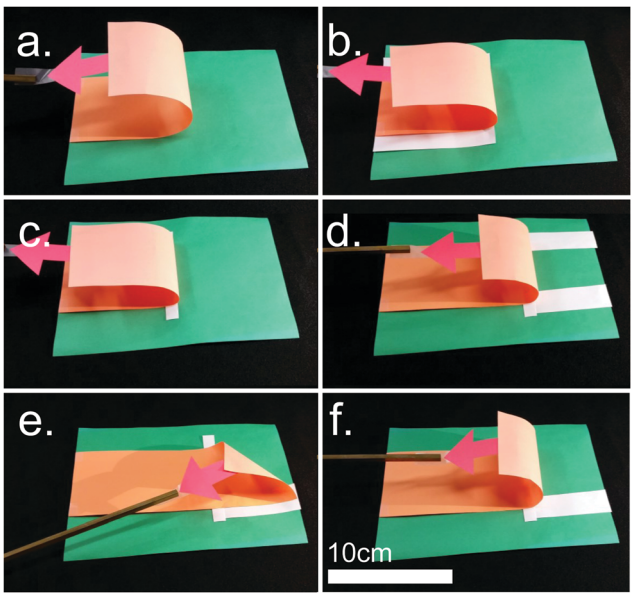

Fig. 6 Demonstrations of how thin strips of adhesive substrate can be used to manipulate the direction of, and amount of capillary peel. Green represents low-adhesion substrate where capillary peel of the film (orange) is possible. White substrate represents areas with high film–substrate adhesion, where capillary forces are lower than adhesive forces when compared directly. Red arrows point in the direction of the capillary force created by the liquid drop. All films are assumed secured on the left side of the setup to ensure peeling occurs on the right. (a) A film that is completely on a low-adhesion substrate will peel until the capillary drop is covered, or there is no film left to peel. (b) A film placed with half of its length on the adhesive substrate will begin by capillary peeling the low-adhesion "free end", and continue peeling until the peel front reaches the area of high adhesion. (c) A thin adhesive strip placed perpendicular to the direction of peel will act similar to a large area of adhesive. Peel will stop as the peel front reaches the adhesive strip and encounters high adhesion along the entire peel front. (d) Two thin adhesive strips running parallel to the peel direction can act as a guide to the direction of peel. (e) Two thin adhesive strips at a right angle from the peel front will allow a triangular peel from the "free" corner. If these strips are large and adhesive, peel will stop in this folded shape. (f) A thin adhesive strip parallel to the usual direction of peel will allow the previous state (e) to progress into the same folded state as the other capillary peel examples.

2.3 "Fixing" structure with adhesion

Creation of complex, multi-step structures requires both pivot points as well as a means to hold structures in place. While directional adhesion can create pivots, self-adhesion is needed to fix structures after the driving capillary fluid evaporates. The capillary peel experiments described above, showed that once a film peels from its substrate it will often form a 180° bend around the capillary drop and continue to peel from the substrate until the fluid is almost entirely covered with film. When the fluid volume is reduced, it is likely that the film will come into contact with itself, rather than simply opening to the flat state.[47] The result of the film folding onto itself in the presence of adhesion between the film and itself, Fig. 2d, is the creation of a "racquet" shape structure. The structure is stable if the film–film adhesion outweighs the elastic energy stored in the bend. The racquet shape has been studied by various methods with respect to carbon nanotubes and graphene sheets in the absence of water[35–38,48–52] and in capillary origami systems.[26,47,53]

The conditions for a stable racquet shape come down to a balance between adhesion and bending and so must be related to the elastocapillary length L_{ec}. Practically speaking, it is useful to focus on the length of a film which can easily be controlled. A film shorter than some critical length, L_{crit}, will have to create a high curvature bend in order to come into self contact and adhesion will not be strong enough to hold the structure closed. On the other hand, a sheet longer than L_{crit} will not need to have as high a curvature and adhesion will hold it closed. Detailed models describing the film as an Elastica with a two-dimensional cross-section yield more quantitative predictions.[37,38,53] In particular, the critical length is given as

$$L_{crit} = \alpha\sqrt{\frac{B}{\gamma}} \tag{9}$$

where α is a numerical factor determined by the exact model used.

In order to validate eqn (9), we have conducted a set of experiments with PDMS films (see Section 1.4 for details). In short, films are placed on a two phase substrate, such that a certain length lies on a low adhesion directional substrate and the rest of a film lies on a full adhesion substrate. In this way, the free length is easily measured before water is applied to fold the film, and its shape is easily observed after the water is removed.

Fig. 7 shows the summary of these experiments. The solid vertical line indicates the critical thickness for capillary bending determined earlier. In this case, experiments can be conducted at greater thicknesses by circumventing the capillary drop and simply folding the films by hand and placing the free film on top of a capillary drop which is then allowed to dry

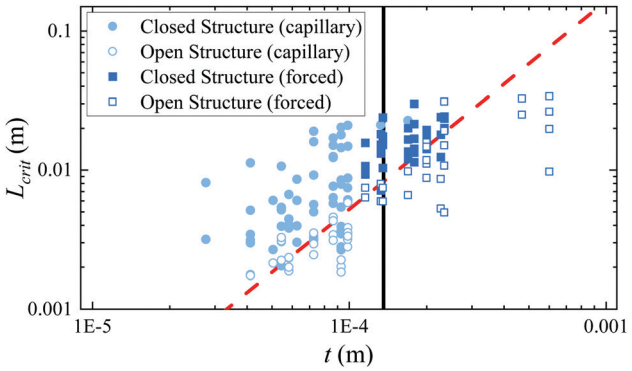

Fig. 7 Experimental results for the racquet stability experiments comparing the length of peeled film (L_{crit}) to the film thickness (t) for open and closed racquet shapes. Solid symbols represent experiments where the closed (racquet-shaped) structure was stable. Open symbols represent experiments where the film released from its folded state and relaxed to its open structure. Experiments where only capillary forces were used to facilitate folding are represented by circles. Squares represent experiments where the film was manually lifted, bent, and placed upon the capillary liquid. The vertical black line largely separating these two situations is at a limiting thickness of 110 μm from eqn (10). The dashed line represents our fit of eqn (9) with α = 3.8.

(solid squares and open squares). It is possible that the film weight affects some of this data. Films folded by capillary action alone are shown as solid and open circles. In both cases we see the transition between stable racquet shapes (solid symbols) and open flat shapes (open symbols) falls along a straight line (in this log/log plot). Fitting eqn (9) yields an α value of 3.8, which is consistent with the original measurements of Py and Bico (α = 4.9) and modelling of Liu *et al.* (α = 3.03).[26,53] It is important to note that a higher value of α is predicted by considering the overall system energy (α = 12.11 by Liu *et al.* and $\alpha = 4\pi$ by Zhou *et al.*), but is not observed here.[37,53]

2.4 Double folding

A critical feature of any complete system of origami assembly is the requirement that it be possible for the sheet to be folded multiple consecutive times. The combination of directional patterned adhesion and self-adhesion which can fix bends in place allows adhesive capillary origami to meet this basic need. We demonstrate the formation and fixation of a double fold, the most basic example of a consecutive fold, in Fig. 8.

In Fig. 8a, a square film is shown resting on a patterned substrate. The substrate is made up of four patterned blocks arranged such that the top two quadrants have a vertical line pattern, the lower right quadrant has a horizontal line pattern and the lower left quadrant is unpatterned. In addition, the lower right quadrant is bordered top and bottom with two wide adhesive strips (adhesive areas highlighted in ESI†). These strips were necessary to stop the lower right corner from peeling when water is first introduced to the system.

As water is added to the center of the film, the top half of the film easily peels from the substrate forming the first fold (Fig. 8b). Occasionally, folds were observed to occur so rapidly that the momentum of the water and film moving to the half

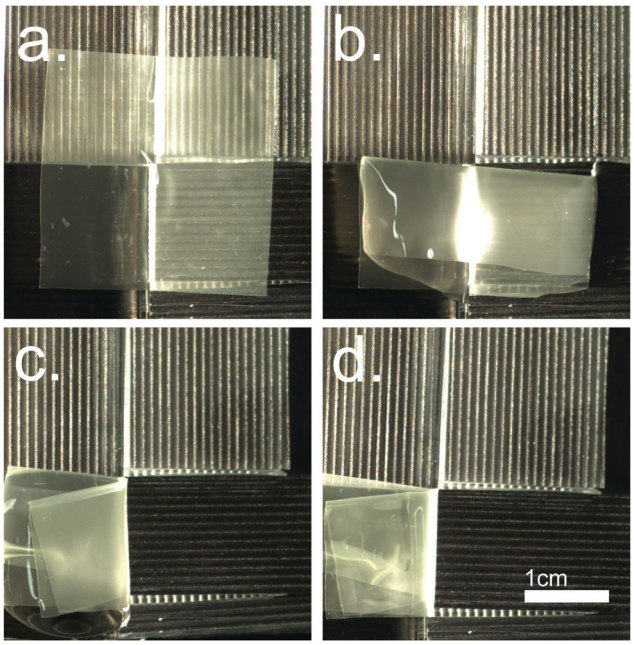

Fig. 8 Sequence of capillary folding a flat sheet into a double-fold configuration. (a) Thin film laying on a patterned substrate. The bottom-left quadrant and two thin, horizontal strips in the bottom-right quadrant are fully adhered to the substrate. Other areas are on substrates with very low film adhesion. (b) Water was added to the center of the film and facilitated a peel and folded the sheet in half. As the film dried, the fold was made permanent. (c) Water was added to the center of the top of the single-folded sheet to facilitate the second fold. Capillary peel was strong enough to not only peel the double thick film, but to also peel the film from the thin strip of full adhesion. (d) After all of the water disappears, the double-fold is stable.

bent state pushed the peel front past the thin horizontal adhesive strip at the top of the lower right quadrant. The system did not fall into an undesirable deformation because the half folded state is the lowest energy state. So long as the lower right quadrant holds as the fold is initiated the desired symmetry is achieved. The momentum effect has the added benefit of making peeling of later stages easier but is also, to some degree, less predictable. We focus on low momentum experiments for simplicity.

After the first fold has been formed, we withdraw the large water drop with a syringe. The water could be left to evaporate without altering the outcome, but the syringe is used to speed the experiment. Once self-contact occurs, the film remains in this half-folded state indefinitely as its length is many times larger than L_{crit}. Critically, the self-adhesion allows water to be added to the film to initiate the second fold. The second water drop cannot initiate a peel front anywhere on the full adhesion quadrant, so peeling from the right end of the film is the only option. The film then folds in half again, this time the right side folding on top of the left (Fig. 8c). Again, water is withdrawn to fix the double fold through self-adhesion, resulting in a folded area one quarter that of the initial sheet.

We can again estimate the energies involved in bending the film the second time (steps (b) to (c) in Fig. 8). Clearly the fluid

has not changed, but now the film is harder to bend because it is effectively twice as thick as it was during the first folding step.[54,55] From this point of view we need change the thickness in eqn (3), which ultimately moves our limiting thickness down to smaller levels. Explicitly, we find the limit to now be given by:

$$t_{\Delta\gamma\to 0} = \left[\frac{3R^2\Delta\gamma'\left(1-\nu^2\right)}{E}\right]^{\frac{1}{3}}. \qquad (10)$$

From an alternative point of view, the elastocapillary length grows by a factor of $2^{3/2}$ for each additional 'level' of folding. We note that the true cost will be slightly underestimated here because we ignore the cost of the d-cone formed at the intersection of the initial and secondary fold axis (the top right corner in Fig. 8).

This process is quite repeatable for a square sheet that is placed so the area of the sheet in each quadrant is equal. A capillary drop placed in the center of the flat sheet and added to until the first fold occurs in this configuration will reliably fold the top half onto the bottom half. An initial peel initiated at one of the top corners of the sheet will advance until it encounters one of the high-adhesion areas, which then acts as a pivot point securing an edge of the peel front and progressing until the entirety of the top quadrants have peeled. After the fold initiates, adding water until the entirety of the unpeeled sheet is covered allows the fold to progress to the furthest extent of covering the bottom sheet. Ensuring that the bottom-rightmost corner of the film is adhered to a thin adhesive strip stops peels from initiating in that corner. Occasional miss-folds would occur when the top right corner initiated peeling in a very quick manner. Effectively peeling through the adhesive strip separating the two right quadrants and leading to a diagonal fold where the top right half of the film would fold onto the bottom left half of the film. This could be avoided by adding the water drop more towards the left side of the film, or slowing down the addition of water to ensure there weren't large and fast folds. The second fold typically initiates at a corner on the right side of the film and peels from the thin strips individually. Again, water is added to cover the bottom left quadrant to allow the fold to cover the entire quadrant.

2.5 Construction of complex structures

The steps needed to create complex structures using thin-film capillary origami have now been described in this paper, however, a clear demonstration of a functional, complex design is still lacking. The paper airplane is a less academically motivated structure, but is familiar to many who have been bored and had a piece of paper nearby. The airplane also represents an origami designed to have additional functionality, in this case gliding ability. The folding procedure required to make this structure is well-known and gives a good bridge between the discussion of basic physical guidelines and practical application of processes in a complex design.

The initial step requires peeling from the substrate and folding two corners of a sheet in to meet along the sheet's center line. Next, the sheet is folded along the center line. Both

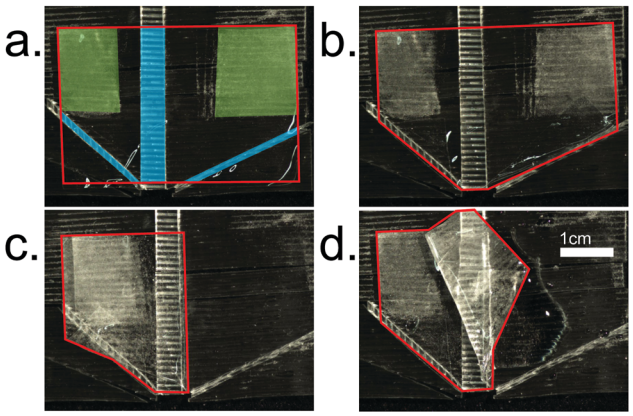

Fig. 9 The major steps in the process of capillary folding of an airplane shape. In each step the outline of the shape is drawn in red to distinguish the clear PDMS sheet from the patterned PDMS substrate. (a) Thin film placed upon patterned substrate. Areas highlighted in blue have high film–substrate adhesion and have been coated with a water-soluble release layer. All other areas have low film–substrate adhesion. Areas highlighted in green have a nonstick coating applied to the top of the film, acting as a low adhesion area when the film contacts itself. (b) The corners of the film have been folded in, forming the nose of the airplane. (c) The right wing has been folded over the left wing, forming the backbone of the airplane. (d) The right wing has been partially unfolded from the left wing, completing the multi-step folding process to create a stable airplane shape. Further application of water under the airplane releases it from the substrate.

these steps can proceed with an appropriately patterned substrate and two sequential drop placement and drying steps. However, the final step is to peel the wings apart and give the airplane its glider shape. This step required a modified implementation of the principles discussed earlier. In this case the sheet itself must also be patterned to facilitate a low self-adhesion between the wings. Specifically, here the wing tops were treated with a hard PS particle layer which reduced adhesion much like dirtying a piece of tape. This area is highlighted in green in Fig. 9a. The final structure is shown in a floating state (to release it from its substrate) outlined in red in Fig. 9d. A video with the intermediate steps is available in ESI.†

The airplane represents construction of a multi-step, complex, and stable structure using only capillary origami techniques demonstrating a realistic further development of guided self assembly with thin-films. The basic actions of origami – lifting, folding, creasing, and unfolding – have all been recreated with the tools of capillarity and adhesion. These new tools have expanded the library of what is possible, and point the way for the possibility of even greater innovation in the future through the many modifications to adhesion and capillarity currently available (switchable adhesion, use of different liquids, patterned changes in wetting, time dependent capillarity, and so on).

3 Conclusions

This work has provided a simple summary of the role of adhesion in capillary peeling of thin films. The lift created by

the surface tension of a drop must exceed the cost of adhesion between a film and a substrate in order for origami to be possible. Furthermore, if the substrate adhesion is anisotropic, folding can be guided in a symmetry breaking manner. Further, mechanisms can be created through self-adhesion which allow a film to be folded in a sequential manner. Without adhesion complex origami could not be assembled by fluid droplets.

We have demonstrated the balance between capillary lift caused by a fluid's surface tension and the adhesion between a sheet and its substrate. A PDMS sheet must have a substrate adhesion lower than 0.38 in order for water to lift it from its substrate. Additionally, the film must be thinner than 110 μm or it cannot bend around a water droplet. Similarly, a film must have a length greater than L_{crit} in order to come into self-contact and maintain a fold after the water has completely dried. Combining these rules, we demonstrate a sequentially doubly folded sheet, a critical step towards complex guided self-assembly in this system. Finally, we have demonstrated a more detailed structure by assembling a paper airplane from a sheet with only water drops, guided adhesion and self-adhesion.

This work not only highlights what is currently possible for adhesion-controlled capillary origami, but opens the door for many possible variations in the basic technology. Adhesion, for example, is a well-studied concept and many innovations have been created over the years which could be combined with a thin sheet. For example, adhesive layers which are responsive to the environment could easily be patterned on sheets in order to create reversible or multi-state structures. Surfactant patches could be added in order to rapidly drop surface tension once a drop reaches the patch. Fluid mixtures could be utilized to create dynamic surface tensions, or to create or alter adhesion during folding. Finally, electronic response such as in electrowetting could be used to drive origami between different states of assembly, and allow for more complex soft robotics applications.[56,57]

Conflicts of interest

There are no conflicts to declare.

Acknowledgements

Special thanks to Paul Omernik and the North Dakota State University Department of Physics for providing expertise and materials for the 3D printing of moulds used in experiments. The authors gratefully acknowledge the support of the National Science Foundation through grant number CMMI-2011681.

Notes and references

1 W. Wu and Z. You, *Proc. R. Soc. A*, 2011, **467**, 2561–2574.
2 A. Malczyk and H.-D. Adomeit, *SAE Trans.*, 1995, 2890–2906.
3 R. J. Lang, *Phys. World*, 2007, **20**, 30.
4 E. A. Peraza-Hernandez, D. J. Hartl, R. J. Malak Jr and D. C. Lagoudas, *Smart Mater. Struct.*, 2014, **23**, 094001.
5 N. Turner, B. Goodwine and M. Sen, *Proc. Inst. Mech. Eng., Part C*, 2016, **230**, 2345–2362.
6 R. Tang, H. Huang, H. Tu, H. Liang, M. Liang, Z. Song, Y. Xu, H. Jiang and H. Yu, *Appl. Phys. Lett.*, 2014, **104**, 083501.
7 T. Chen, O. R. Bilal, R. Lang, C. Daraio and K. Shea, *Phys. Rev. Appl.*, 2019, **11**, 064069.
8 H. Yasuda, Y. Miyazawa, E. G. Charalampidis, C. Chong, P. G. Kevrekidis and J. Yang, *Sci. Adv.*, 2019, **5**, eaau2835.
9 S. Li, D. M. Vogt, D. Rus and R. J. Wood, *Proc. Natl. Acad. Sci. U. S. A.*, 2017, **114**, 13132–13137.
10 J. Rogers, Y. Huang, O. G. Schmidt and D. H. Gracias, *MRS Bull.*, 2016, **41**, 123–129.
11 Z. Song, T. Ma, R. Tang, Q. Cheng, X. Wang, D. Krishnaraju, R. Panat, C. K. Chan, H. Yu and H. Jiang, *Nat. Commun.*, 2014, **5**, 1–6.
12 S.-J. Cho, K.-H. Choi, J.-T. Yoo, J.-H. Kim, Y.-H. Lee, S.-J. Chun, S.-B. Park, D.-H. Choi, Q. Wu and S.-Y. Lee, *et al.*, *Adv. Funct. Mater.*, 2015, **25**, 6029–6040.
13 K. Kuribayashi, K. Tsuchiya, Z. You, D. Tomus, M. Umemoto, T. Ito and M. Sasaki, *Mater. Sci. Eng., A*, 2006, **419**, 131–137.
14 J.-H. Na, N. P. Bende, J. Bae, C. D. Santangelo and R. C. Hayward, *Soft Matter*, 2016, **12**, 4985–4990.
15 J. Bae, N. P. Bende, A. A. Evans, J.-H. Na, C. D. Santangelo and R. C. Hayward, *Mater. Horiz.*, 2017, **4**, 228–235.
16 S.-J. Jeon and R. C. Hayward, *Soft Matter*, 2020, **16**, 688–694.
17 J.-H. Cho and D. H. Gracias, *Nano Lett.*, 2009, **9**, 4049–4052.
18 J.-H. Cho, M. D. Keung, N. Verellen, L. Lagae, V. Moshchalkov, P. Van Dorpe and D. H. Gracias, *Small*, 2011, **7**, 1943–1948.
19 S. Chen, J. Chen, X. Zhang, Z.-Y. Li and J. Li, *Light: Sci. Appl.*, 2020, **9**, 1–19.
20 M. Z. Miskin, K. J. Dorsey, B. Bircan, Y. Han, D. A. Muller, P. L. McEuen and I. Cohen, *Proc. Natl. Acad. Sci. U. S. A.*, 2018, **115**, 466–470.
21 M. F. Reynolds, K. L. McGill, M. A. Wang, H. Gao, F. Mujid, K. Kang, J. Park, M. Z. Miskin, I. Cohen and P. L. McEuen, *Nano Lett.*, 2019, **19**, 6221–6226.
22 B. Bircan, M. Z. Miskin, R. J. Lang, M. C. Cao, K. J. Dorsey, M. G. Salim, W. Wang, D. A. Muller, P. L. McEuen and I. Cohen, *Nano Lett.*, 2020, **20**, 4850–4856.
23 A. Azam, K. E. Laflin, M. Jamal, R. Fernandes and D. H. Gracias, *Biomed. Microdevices*, 2011, **13**, 51–58.
24 R. Fernandes and D. H. Gracias, *Adv. Drug Delivery Rev.*, 2012, **64**, 1579–1589.
25 M. Johnson, Y. Chen, S. Hovet, S. Xu, B. Wood, H. Ren, J. Tokuda and Z. T. H. Tse, *Int. J. Comput. Assist. Radiol. Surg.*, 2017, **12**, 2023–2032.
26 C. Py, P. Reverdy, L. Doppler, J. Bico, B. Roman and C. N. Baroud, *Phys. Rev. Lett.*, 2007, **98**, 156103.
27 J. Bico, B. Roman, L. Moulin and A. Boudaoud, *Nature*, 2004, **432**, 690.
28 K. S. Kwok, Q. Huang, M. Mastrangeli and D. H. Gracias, *Adv. Mater. Interfaces*, 2020, **7**, 1901677.
29 D. H. Gracias, V. Kavthekar, J. C. Love, K. E. Paul and G. M. Whitesides, *Adv. Mater.*, 2002, **14**, 235–238.

30 T. G. Leong, P. A. Lester, T. L. Koh, E. K. Call and D. H. Gracias, *Langmuir*, 2007, **23**, 8747–8751.
31 C. L. Randall, E. Gultepe and D. H. Gracias, *Trends Biotechnol.*, 2012, **30**, 138–146.
32 A. Legrain, T. Janson, J. W. Berenschot, L. Abelmann and N. R. Tas, *J. Appl. Phys.*, 2014, **115**, 214905.
33 A. Legrain, J. W. Berenschot, N. R. Tas and L. Abelmann, *Microelectron. Eng.*, 2015, **140**, 60–66.
34 R. J. Lang, *Origami and geometric constructions*, Self Published, (1996, 2003), 1996.
35 X. Chen, L. Zhang, Y. Zhao, X. Wang and C. Ke, *J. Appl. Phys.*, 2014, **116**, 164301.
36 X.-H. Meng, M. Li, Z. Kang, X. Z. Zhang and J.-L. Xiao, *J. Phys. D: Appl. Phys.*, 2013, **46**, 055308.
37 W. Zhou, Y. Huang, B. Liu, K. Hwang, J. Zuo, M. Buehler and H. Gao, *Appl. Phys. Lett.*, 2007, **90**, 073107.
38 N. Glassmaker and C. Hui, *J. Appl. Phys.*, 2004, **96**, 3429–3434.
39 T. Elder, T. Twohig, H. Singh and A. B. Croll, *Soft Matter*, 2020, **16**, 10611–10619.
40 A. Antkowiak, B. Audoly, C. Josserand, S. Neukirch and M. Rivetti, *Proc. Natl. Acad. Sci. U. S. A.*, 2011, **108**, 10400–10404.
41 D. Maugis and M. Barquins, *Adhesion and adsorption of polymers*, Springer, 1980, pp. 203–277.
42 K. R. Shull, *Mater. Sci. Eng., R*, 2002, **36**, 1–45.
43 K. Efimenko, W. E. Wallace and J. Genzer, *J. Colloid Interface Sci.*, 2002, **254**, 306–315.
44 R. W. Style, R. Boltyanskiy, Y. Che, J. Wettlaufer, L. A. Wilen and E. R. Dufresne, *Phys. Rev. Lett.*, 2013, **110**, 066103.
45 T. Twohig, S. May and A. B. Croll, *Soft Matter*, 2018, **14**, 7492–7499.
46 P.-G. De Gennes, F. Brochard-Wyart and D. Quéré, *Capillarity and wetting phenomena: drops, bubbles, pearls, waves*, Springer Science & Business Media, 2013.
47 N. D. Brubaker, *SIAM J. Appl. Math.*, 2019, **79**, 572–593.
48 O. G. Schmidt and K. Eberl, *Nature*, 2001, **410**, 168.
49 X.-H. Meng, M. Li, Z. Kang and J.-L. Xiao, *Acta Mech. Sin.*, 2014, **30**, 410–417.
50 S. Cranford, D. Sen and M. J. Buehler, *Appl. Phys. Lett.*, 2009, **95**, 123121.
51 B. J. Cox, D. Baowan, W. Bacsa and J. B. Hill, *RSC Adv.*, 2015, **5**, 57515.
52 J. Aljedani, M. J. Chen and B. J. Cox, *Mater. Res. Express*, 2021, **8**, 015002.
53 J. Liu and J. H. Lee, *J. Mech. Mater. Struct.*, 2013, **8**, 169–183.
54 T. Elder, D. Rozairo and A. B. Croll, *Macromolecules*, 2019, **52**, 690–699.
55 S. Deboeuf, E. Katzav, A. Boudaoud, D. Bonn and M. Adda-Bedia, *Phys. Rev. Lett.*, 2013, **110**, 104301.
56 Y. Li, R. Chen and R. J. Baker, *IEEE 57th International Midwest Symposium on Circuits and Systems (MWSCAS)*, 2014, pp. 326–329.
57 F. Song, L. Ma, J. Fan, Q. Chen, G. Lei and B. Q. Li, *Phys. Chem. Chem. Phys.*, 2018, **20**, 11987–11993.

